Article:

Abed Abud, A, Abi, B, Acciarri, R et al. (2022) Separation of track- and shower-like energy deposits in ProtoDUNE-SP using a convolutional neural network. European Physical Journal C, 82 (10). 903. ISSN: 1434-6044

https://doi.org/10.1140/epjc/s10052-022-10791-2

Eur. Phys. J. C (2022) 82:903
https://doi.org/10.1140/epjc/s10052-022-10791-2

THE EUROPEAN PHYSICAL JOURNAL C

Regular Article - Experimental Physics

Separation of track- and shower-like energy deposits in ProtoDUNE-SP using a convolutional neural network

DUNE Collaboration

A. Abed Abud[36,127], B. Abi[155], R. Acciarri[67], M. A. Acero[11], M. R. Adames[191], G. Adamov[72], M. Adamowski[67], D. Adams[21], M. Adinolfi[20], A. Aduszkiewicz[81], J. Aguilar[125], Z. Ahmad[202], J. Ahmed[205], B. Aimard[53], B. Ali-Mohammadzadeh[32,93], T. Alion[189], K. Allison[44], S. Alonso Monsalve[36,60], M. AlRashed[117], C. Alt[60], A. Alton[12], R. Alvarez[40], P. Amedo[86], J. Anderson[7], C. Andreopoulos[127,176], M. Andreotti[68,94], M. Andrews[67], F. Andrianala[5], S. Andringa[126], N. Anfimov[115], A. Ankowski[181], M. Antoniassi[191], M. Antonova[85], A. Antoshkin[115], S. Antusch[14], A. Aranda-Fernandez[43], L. Arellano[133], L. O. Arnold[46], M. A. Arroyave[59], J. Asaadi[194], L. Asquith[189], A. Aurisano[41], V. Aushev[123], D. Autiero[108], V. Ayala Lara[103], M. Ayala-Torres[42], F. Azfar[155], M. Babicz[36], A. Back[91], H. Back[156], J. J. Back[205], C. Backhouse[200], I. Bagaturia[72], L. Bagby[67], N. Balashov[115], S. Balasubramanian[67], P. Baldi[25], B. Baller[67], B. Bambah[82], F. Barao[110,126], G. Barenboim[85], G. Barker[205], W. Barkhouse[147], C. Barnes[137], G. Barr[155], J. Barranco Monarca[77], A. Barros[191], N. Barros[61,126], J. L. Barrow[134], A. Basharina-Freshville[200], A. Bashyal[7], V. Basque[133], C. Batchelor[58], E. Batista das Chagas[31], J. Battat[206], F. Battisti[155], F. Bay[4], M. C. Q. Bazetto[31], J. Bazo Alba[168], J. F. Beacom[152], E. Bechetoille[108], B. Behera[45], C. Beigbeder[159], L. Bellantoni[67], G. Bellettini[166], V. Bellini[32,93], O. Beltramello[36], N. Benekos[36], C. Benitez Montiel[9], F. Bento Neves[126], J. Berger[45], S. Berkman[67], P. Bernardini[96,177], R. M. Berner[15], A. Bersani[95], S. Bertolucci[18,92], M. Betancourt[67], A. Betancur Rodríguez[59], A. Bevan[171], Y. Bezawada[24], T. S. Bezerra[189], A. Bhardwaj[129], V. Bhatnagar[158], M. Bhattacharjee[89], D. Bhattarai[143], S. Bhuller[20], B. Bhuyan[89], S. Biagi[102], J. Bian[25], M. Biassoni[97], K. Biery[67], B. Bilki[16,106], M. Bishai[21], A. Bitadze[133], A. Blake[124], F. Blaszczyk[67], G. Blazey[148], E. Blucher[38], J. Boissevain[128], S. Bolognesi[35], T. Bolton[117], L. Bomben[97,105], M. Bonesini[97,139], M. Bongrand[159], C. Bonilla-Diaz[33], F. Bonini[21], A. Booth[171], F. Boran[16], S. Bordoni[36], A. Borkum[189], N. Bostan[150], P. Bour[50], C. Bourgeois[159], D. Boyden[148], J. Bracinik[17], D. Braga[67], D. Brailsford[124], A. Branca[97], A. Brandt[194], J. Bremer[36], D. Breton[159], C. Brew[176], S. J. Brice[67], C. Brizzolari[97,139], C. Bromberg[138], J. Brooke[20], A. Bross[67], G. Brunetti[97,139], M. Brunetti[205], N. Buchanan[45], H. Budd[173], I. Butorov[115], I. Cagnoli[18,92], T. Cai[212], D. Caiulo[108], R. Calabrese[68,94], P. Calafiura[125], J. Calcutt[153], M. Calin[22], S. Calvez[45], E. Calvo[40], A. Caminata[95], M. Campanelli[200], D. Caratelli[67], D. Carber[45], J. Carceller[200], G. Carini[21], B. Carlus[108], M. F. Carneiro[21], P. Carniti[97], I. Caro Terrazas[45], H. Carranza[194], T. Carroll[209], J. F. Castaño Forero[6], A. Castillo[179], C. Castromonte[103], E. Catano-Mur[208], C. Cattadori[97], F. Cavalier[159], G. Cavallaro[97], F. Cavanna[67], S. Centro[100,157], G. Cerati[67], A. Cervelli[92], A. Cervera Villanueva[85], M. Chalifour[36], A. Chappell[205], E. Chardonnet[160], N. Charitonidis[36], A. Chatterjee[167], S. Chattopadhyay[202], M. Chavarry Neyra[103], H. Chen[21], M. Chen[25], Y. Chen[15], Z. Chen[186], Z. Chen-Wishart[174], Y. Cheon[199], D. Cherdack[81], C. Chi[46], S. Childress[67], R. Chirco[87], A. Chiriacescu[22], G. Chisnall[189], K. Cho[120], S. Choate[148], D. Chokheli[72], P. S. Chong[163], A. Christensen[45], D. Christian[67], G. Christodoulou[36], A. Chukanov[115], M. Chung[199], E. Church[156], V. Cicero[18,92], P. Clarke[58], G. Cline[125], T. E. Coan[185], A. G. Cocco[99], J. Coelho[160], N. Colton[45], E. Conley[56], R. Conley[181], J. Conrad[134], M. Convery[181], S. Copello[95], P. Cova[98,161], L. Cremaldi[143], L. Cremonesi[171], J. I. Crespo-Anadón[40], M. Crisler[67], E. Cristaldo[9], J. Crnkovic[143], R. Cross[123], A. Cudd[44], C. Cuesta[40], Y. Cui[27], D. Cussans[20], O. Dalager[25], H. Da Motta[34], L. Da Silva Peres[66], C. David[67,212], Q. David[108], G. S. Davies[143], S. Davini[95], J. Dawson[160], K. De[194], S. De[2], P. Debbins[106], I. De Bonis[53], M. Decowski[3,146], A. De Gouvea[149], P. C. De Holanda[31], I. L. De Icaza Astiz[189], A. Deisting[174], P. De Jong[3,146], A. Delbart[35], D. Delepine[77], M. Delgado[97,139], A. Dell'Acqua[36], N. Delmonte[98,161], P. De Lurgio[7], J. R. De Mello Neto[66], D. M. DeMuth[201], S. Dennis[30], C. Densham[176], G. W. Deptuch[21], A. De Roeck[36], V. De Romeri[85], G. De Souza[31], R. Devi[112], R. Dharmapalan[80], M. Dias[198], F. Diaz[168], J. Diaz[91], S. Di Domizio[71,95], L. Di Giulio[36], P. Ding[67], L. Di Noto[71,95], G. Dirkx[88], C. Distefano[102], R. Diurba[142], M. Diwan[21], Z. Djurcic[7], D. Doering[181], S. Dolan[36], F. Dolek[16], M. Dolinski[55], L. Domine[181], Y. Donon[36], D. Douglas[138], D. Douillet[159], A. Dragone[181], G. Drake[67], F. Drielsma[181], L. Duarte[198], D. Duchesneau[53], K. Duffy[67], P. Dunne[88], B. Dutta[192], H. Duyang[182], O. Dvornikov[80], D. Dwyer[125], A. Dyshkant[148], M. Eads[148], A. Earle[189], D. Edmunds[138],

J. Eisch[67], L. Emberger[133,135], S. Emery[35], P. Englezos[175], A. Ereditato[210], T. Erjavec[24], C. Escobar[67], G. Eurin[35],
J. J. Evans[133], E. Ewart[91], A. C. Ezeribe[180], K. Fahey[67], A. Falcone[97,139], M. Fani’[128], C. Farnese[100], Y. Farzan[109],
D. Fedoseev[115], J. Felix[77], Y. Feng[107], E. Fernandez-Martinez[131], P. Fernandez Menendez[85],
M. Fernandez Morales[86], F. Ferraro[71,95], L. Fields[150], P. Filip[49], F. Filthaut[146,172], M. Fiorini[68,94], V. Fischer[107],
R. S. Fitzpatrick[137], W. Flanagan[52], B. Fleming[210], R. Flight[173], S. Fogarty[45], W. Foreman[87], J. Fowler[56], W. Fox[91],
J. Franc[50], K. Francis[148], D. Franco[210], J. Freeman[67], J. Freestone[133], J. Fried[21], A. Friedland[181],
F. Fuentes Robayo[20], S. Fuess[67], I. K. Furic[69], K. Furman[71], A. P. Furmanski[142], A. Gabrielli[92], A. Gago[168],
H. Gallagher[197], A. Gallas[159], A. Gallego-Ros[40], N. Gallice[98,140], V. Galymov[108], E. Gamberini[36], T. Gamble[180],
F. Ganacim[191], R. Gandhi[78], R. Gandrajula[138], F. Gao[167], S. Gao[21], D. Garcia-Gamez[73], M. Á. García-Peris[85],
S. Gardiner[67], D. Gastler[19], J. Gauvreau[151], G. Ge[46], N. Geffroy[53], B. Gelli[31], A. Gendotti[60], S. Gent[184],
Z. Ghorbani-Moghaddam[95], P. Giammaria[31], T. Giammaria[68,94], N. Giangiacomi[196], D. Gibin[100,157],
I. Gil-Botella[40], S. Gilligan[153], C. Girerd[108], A. Giri[90], D. Gnani[125], O. Gogota[123], M. Gold[144], S. Gollapinni[128],
K. Gollwitzer[67], R. A. Gomes[63], L. Gomez Bermeo[179], L. S. Gomez Fajardo[179], F. Gonnella[17], D. Gonzalez-Diaz[86],
M. Gonzalez-Lopez[131], M. C. Goodman[7], O. Goodwin[133], S. Goswami[165], C. Gotti[97], E. Goudzovski[17], C. Grace[125],
R. Gran[141], E. Granados[77], P. Granger[35], A. Grant[54], C. Grant[19], D. Gratieri[70], P. Green[133], L. Greenler[209],
J. Greer[20], J. Grenard[36], C. Griffith[189], M. Groh[45], J. Grudzinski[7], K. Grzelak[204], W. Gu[21], E. Guardincerri[128],
V. Guarino[7], M. Guarise[68,94], R. Guenette[79], E. Guerard[159], M. Guerzoni[92], D. Guffanti[98], A. Guglielmi[100],
B. Guo[182], A. Gupta[181], V. Gupta[146], K. Guthikonda[121], R. Gutierrez[6], P. Guzowski[133], M. M. Guzzo[31], S. Gwon[39],
C. Ha[39], K. Haaf[67], A. Habig[141], H. Hadavand[194], R. Haenni[15], A. Hahn[67], J. Haiston[183], P. Hamacher-Baumann[155],
T. Hamernik[67], P. Hamilton[88], J. Han[167], D. A. Harris[67,212], J. Hartnell[189], T. Hartnett[176], J. Harton[45],
T. Hasegawa[119], C. Hasnip[155], R. Hatcher[67], K. W. Hatfield[25], A. Hatzikoutelis[178], C. Hayes[91], K. Hayrapetyan[171],
J. Hays[171], E. Hazen[19], M. He[81], A. Heavey[67], K. M. Heeger[210], J. Heise[188], S. Henry[173],
M. Hernandez Morquecho[87], K. Herner[67], J. Hewes[41], C. Hilgenberg[142], T. Hill[83], S. J. Hillier[17], A. Himmel[67],
E. Hinkle[38], L. R. Hirsch[191], J. Ho[79], J. Hoff[67], A. Holin[176], E. Hoppe[156], G. A. Horton-Smith[117], M. Hostert[142],
A. Hourlier[134], B. Howard[67], R. Howell[173], J. Hoyos[136], I. Hristova[176], M. S. Hronek[67], J. Huang[24], Z. Hulcher[181],
G. Iles[88], N. Ilic[196], A. M. Iliescu[92], R. Illingworth[67], G. Ingratta[18,92], A. Ioannisian[211], B. Irwin[142], L. Isenhower[1],
R. Itay[181], C. M. Jackson[156], V. Jain[2], E. James[67], W. Jang[194], B. Jargowsky[25], F. Jediny[50], D. Jena[67], Y. Jeong[39,106],
C. Jesús-Valls[84], X. Ji[21], L. Jiang[203], S. Jiménez[40], A. Jipa[22], R. Johnson[41], W. Johnson[183], N. Johnston[91],
B. Jones[194], S. Jones[200], M. Judah[167], C. Jung[186], T. Junk[67], Y. Jwa[46], M. Kabirnezhad[155], A. Kaboth[174,176],
I. Kadenko[123], I. Kakorin[115], A. Kalitkina[115], D. Kalra[46], F. Kamiya[65], N. Kaneshige[28], D. M. Kaplan[87],
G. Karagiorgi[46], G. Karaman[106], A. Karcher[125], M. Karolak[35], Y. Karyotakis[53], S. Kasai[122], S. P. Kasetti[129],
L. Kashur[45], N. Kazaryan[211], E. Kearns[19], P. Keener[163], K. J. Kelly[36], E. Kemp[31], O. Kemularia[72], W. Ketchum[67],
S. H. Kettell[21], M. Khabibullin[104], A. Khotjantsev[104], A. Khvedelidze[72], D. Kim[192], B. King[67], B. Kirby[46],
M. Kirby[67], J. Klein[163], A. Klustova[88], T. Kobilarcik[67], K. Koehler[209], L. W. Koerner[81], D. H. Koh[181], S. Kohn[23,125],
P. P. Koller[15], L. Kolupaeva[115], D. Korablev[115], M. Kordosky[208], T. Kosc[76], U. Kose[36], V. Kostelecky[91],
K. Kothekar[20], R. Kralik[189], L. Kreczko[20], F. Krennrich[107], I. Kreslo[15], W. Kropp[25], T. Kroupova[163], S. Kubota[79],
Y. Kudenko[104], V. A. Kudryavtsev[180], S. Kulagin[104], J. Kumar[80], P. Kumar[180], P. Kunze[53], N. Kurita[181],
C. Kuruppu[182], V. Kus[50], T. Kutter[129], J. Kvasnicka[49], D. Kwak[199], A. Lambert[125], B. Land[163], C. E. Lane[55],
K. Lang[195], T. Langford[210], M. Langstaff[133], J. Larkin[21], P. Lasorak[189], D. Last[163], A. Laundrie[209], G. Laurenti[92],
A. Lawrence[125], I. Lazanu[22], R. LaZur[45], M. Lazzaroni[98,140], T. Le[197], S. Leardini[86], J. Learned[80], P. LeBrun[108],
T. LeCompte[181], C. Lee[67], S. Lee[114], G. Lehmann Miotto[36], R. Lehnert[91], M. Leigui de Oliveira[65], M. Leitner[125],
L. M. Lepin[133], S. Li[181], Y. Li[21], H. Liao[117], C. Lin[125], Q. Lin[181], S. Lin[129], R. A. Lineros[33], J. Ling[187], A. Lister[209],
B. R. Littlejohn[87], J. Liu[25], Y. Liu[38], S. Lockwitz[67], T. Loew[125], M. Lokajicek[49], I. Lomidze[72], K. Long[88],
T. Lord[205], J. LoSecco[150], W. C. Louis[128], X. Lu[205], K. Luk[23,125], B. Lunday[163], X. Luo[28], E. Luppi[68,94], T. Lux[84],
V. P. Luzio[65], J. Maalmi[159], D. MacFarlane[181], A. Machado[31], P. Machado[67], C. Macias[91], J. Macier[67],
A. Maddalena[75], A. Madera[36], P. Madigan[23,125], S. Magill[7], K. Mahn[138], A. Maio[61,126], A. Major[56],
J. A. Maloney[51], G. Mandrioli[92], R. C. Mandujano[25], J. C. Maneira[61,126], L. Manenti[200], S. Manly[173], A. Mann[197],
K. Manolopoulos[176], M. Manrique Plata[91], V. N. Manyam[21], L. Manzanillas[159], M. Marchan[67], A. Marchionni[67],
W. Marciano[21], D. Marfatia[80], C. Mariani[203], J. Maricic[80], R. Marie[159], F. Marinho[64], A. D. Marino[44],
D. Marsden[133], M. Marshak[142], C. Marshall[173], J. Marshall[205], J. Marteau[108], J. Martin-Albo[85], N. Martinez[117],
D. A. Martinez Caicedo[183], P. Martínez Miravé[85], S. Martynenko[186], V. Mascagna[97,105], K. Mason[197],
A. Mastbaum[175], F. Matichard[125], S. Matsuno[80], J. Matthews[129], C. Mauger[163], N. Mauri[18,92], K. Mavrokoridis[127],
I. Mawby[205], R. Mazza[97], A. Mazzacane[67], E. Mazzucato[35], T. McAskill[206], E. McCluskey[67], N. McConkey[133],

K. S. McFarland[173], C. McGrew[186], A. McNab[133], A. Mefodiev[104], P. Mehta[113], P. Melas[10], O. Mena[85], H. Mendez[169], P. Mendez[36], D. P. Méndez[21], A. Menegolli[101,162], G. Meng[100], M. Messier[91], W. Metcalf[129], T. Mettler[15], M. Mewes[91], H. Meyer[207], T. Miao[67], G. Michna[184], T. Miedema[146,172], V. Mikola[200], R. Milincic[80], G. Miller[133], W. Miller[142], J. Mills[197], O. Mineev[104], A. Minotti[98,139], O. G. Miranda[42], S. Miryala[21], C. Mishra[67], S. Mishra[182], A. Mislivec[142], M. Mitchell[129], D. Mladenov[36], I. Mocioiu[164], K. Moffat[57], N. Moggi[18,92], R. Mohanta[82], T. A. Mohayai[67], N. Mokhov[67], J. A. Molina[9], L. Molina Bueno[85], E. Montagna[18,92], A. Montanari[92], C. Montanari[67,101,162], D. Montanari[67], L. M. Montano Zetina[42], S. Moon[199], M. Mooney[45], A. F. Moor[30], D. Moreno[6], D. Moretti[97], C. Morris[81], C. Mossey[67], M. Mote[129], E. Motuk[200], C. A. Moura[65], J. Mousseau[137], G. Mouster[124], W. Mu[67], L. Mualem[29], J. Mueller[45], M. Muether[207], S. Mufson[91], F. Muheim[58], A. Muir[54], M. Mulhearn[24], D. Munford[81], H. Muramatsu[142], S. Murphy[60], J. Musser[91], J. Nachtman[106], S. Nagu[130], M. Nalbandyan[211], R. Nandakumar[176], D. Naples[167], S. Narita[111], A. Nath[89], A. Navrer-Agasson[133], N. Nayak[25], M. Nebot-Guinot[58], K. Negishi[111], J. K. Nelson[208], J. Nesbit[209], M. Nessi[36], D. Newbold[176], M. Newcomer[163], H. Newton[54], R. Nichol[200], F. Nicolas-Arnaldos[73], A. Nikolica[163], E. Niner[67], K. Nishimura[80], A. Norman[67], A. Norrick[67], R. Northrop[38], P. Novella[85], J. A. Nowak[124], M. Oberling[7], J. Ochoa-Ricoux[25], A. Olivier[173], A. Olshevskiy[115], Y. Onel[106], Y. Onishchuk[123], J. Ott[25], L. Pagani[24], G. Palacio[59], O. Palamara[67], S. Palestini[36], J. M. Paley[67], M. Pallavicini[71,95], C. Palomares[40], W. Panduro Vazquez[174], E. Pantic[24], V. Paolone[167], V. Papadimitriou[67], R. Papaleo[102], A. Papanestis[176], S. Paramesvaran[20], S. Parke[67], E. Parozzi[97,139], Z. Parsa[21], M. Parvu[22], S. Pascoli[18,57], L. Pasqualini[18,92], J. Pasternak[88], J. Pater[133], C. Patrick[200], L. Patrizii[92], R. B. Patterson[29], S. Patton[125], T. Patzak[160], A. Paudel[67], B. Paulos[209], L. Paulucci[65], Z. Pavlovic[67], G. Pawloski[142], D. Payne[127], V. Pec[49], S. J. Peeters[189], A. Pena Perez[181], E. Pennacchio[108], A. Penzo[106], O. L. Peres[31], J. Perry[58], D. Pershey[56], G. Pessina[97], G. Petrillo[181], C. Petta[32,93], R. Petti[181], V. Pia[18,92], F. Piastra[15], L. Pickering[138], F. Pietropaolo[36,100], V. L. Pimentel[31,47], G. Pinaroli[21], K. Plows[155], R. Plunkett[67], R. Poling[142], F. Pompa[85], X. Pons[36], N. Poonthottathil[107], F. Poppi[18,92], S. Pordes[67], J. Porter[189], M. Potekhin[21], R. Potenza[32,93], B. V. Potukuchi[112], J. Pozimski[88], M. Pozzato[18,92], S. Prakash[31], T. Prakash[125], M. Prest[37], S. Prince[79], F. Psihas[67], D. Pugnere[108], X. Qian[21], J. Raaf[67], V. Radeka[21], J. Rademacker[20], B. Radics[60], A. Rafique[7], E. Raguzin[21], M. Rai[205], M. Rajaoalisoa[41], I. Rakhno[67], A. Rakotonandrasana[5], L. Rakotondravohitra[5], R. Rameika[67], M. Ramirez Delgado[163], B. Ramson[67], A. Rappoldi[101,162], G. Raselli[101,162], P. Ratoff[124], S. Raut[186], R. Razakamiandra[5], E. Rea[142], J. Real[76], B. Rebel[67,209], R. Rechenmacher[67], M. Reggiani-Guzzo[133], J. Reichenbacher[183], S. D. Reitzner[67], H. Rejeb Sfar[36], A. Renshaw[81], S. Rescia[21], F. Resnati[36], A. Reynolds[155], M. Ribas[191], S. Riboldi[98], C. Riccio[186], G. Riccobene[102], L. C. Rice[167], J. Ricol[76], A. Rigamonti[36], Y. Rigaut[60], E. V. Rincón[59], H. Ritchie-Yates[174], D. Rivera[128], A. Robert[76], L. Rochester[181], M. Roda[127], P. Rodrigues[155], M. J. Rodriguez Alonso[36], E. Rodriguez Bonilla[6], J. Rodriguez Rondon[183], S. Rosauro-Alcaraz[131], M. Rosenberg[167], P. Rosier[159], B. Roskovec[25], M. Rossella[101,162], M. Rossi[36], J. Rout[113], P. Roy[207], A. Rubbia[60], C. Rubbia[74], B. Russell[125], D. Ruterbories[173], A. Rybnikov[115], A. Saa-Hernandez[86], R. Saakyan[200], S. Sacerdoti[160], T. Safford[138], N. Sahu[90], P. Sala[36,98], N. Samios[21], O. Samoylov[115], M. Sanchez[107], V. Sandberg[128], D. A. Sanders[143], D. Sankey[176], S. Santana[169], M. Santos-Maldonado[169], N. Saoulidou[10], P. Sapienza[102], C. Sarasty[41], I. Sarcevic[8], G. Savage[67], V. Savinov[167], A. Scaramelli[101], A. Scarff[180], A. Scarpelli[21], T. Schefke[129], H. Schellman[67,153], S. Schifano[68,94], P. Schlabach[67], D. Schmitz[38], A. W. Schneider[134], K. Scholberg[56], A. Schukraft[67], E. Segreto[31], A. Selyunin[115], C. R. Senise Jr.[198], J. Sensenig[165], A. Sergi[17], D. Sgalaberna[60], M. Shaevitz[46], S. Shafaq[113], F. Shaker[212], M. Shamma[27], R. Sharankova[197], H. R. Sharma[112], R. Sharma[21], R. K. Sharma[170], T. Shaw[67], K. Shchablo[108], C. Shepherd-Themistocleous[176], A. Sheshukov[115], S. Shin[114], I. Shoemaker[203], D. Shooltz[138], R. Shrock[186], H. Siegel[46], L. Simard[159], J. Sinclair[181], G. Sinev[183], J. Singh[130], J. Singh[130], L. Singh[48], P. Singh[171], V. Singh[13,48], R. Sipos[36], F. Sippach[46], G. Sirri[92], A. Sitraka[183], K. Siyeon[39], K. Skarpaas[181], A. Smith[30], E. Smith[91], P. Smith[91], J. Smolik[50], M. Smy[25], E. Snider[67], P. Snopok[87], D. Snowden-Ifft[151], M. Soares Nunes[190], H. Sobel[25], M. Soderberg[190], S. Sokolov[115], C. J. Solano Salinas[103], S. Söldner-Rembold[133], S. Soleti[125], N. Solomey[207], V. Solovov[126], W. E. Sondheim[128], M. Sorel[85], A. Sotnikov[115], J. Soto-Oton[40], F. Soto Ugaldi[103], A. Sousa[41], K. Soustruznik[37], F. Spagliardi[155], M. Spanu[97,139], J. Spitz[137], N. J. C. Spooner[180], K. Spurgeon[190], M. Stancari[67], L. Stanco[100,157], C. Stanford[79], D. Stefan[36], R. Stein[20], H. Steiner[125], A. F. Steklain Lisbôa[191], J. Stewart[21], B. Stillwell[38], J. Stock[183], F. Stocker[36], T. Stokes[129], M. Strait[142], T. Strauss[67], L. Strigari[192], A. Stuart[43], J. G. Suarez[59], J. Suárez Sunción[103], R. Sulej[67,154], H. Sullivan[194], D. Summers[143], A. Surdo[96], V. Susic[14], L. Suter[67], C. Sutera[32,93], R. Svoboda[24], B. Szczerbinska[193], A. M. Szelc[58], H. Tanaka[181], S. Tang[21], A. Tapia[136], B. Tapia Oregui[195], A. Tapper[88], S. Tariq[67], E. Tarpara[21], N. Tata[79], E. Tatar[83], R. Tayloe[91], A. Teklu[186], P. Tennessen[4,125], M. Tenti[92], K. Terao[181], C. A. Ternes[85], F. Terranova[97,139], G. Testera[95], T. Thakore[41], A. Thea[176],

J. L. Thompson[180], C. Thorn[21], S. Timm[67], V. Tishchenko[21], L. Tomassetti[68,94], A. Tonazzo[160], D. Torbunov[142], M. Torti[97,139], M. Tortola[85], F. Tortorici[32,93], N. Tosi[92], D. Totani[28], M. Toups[67], C. Touramanis[127], R. Travaglini[92], J. Trevor[29], S. Trilov[20], W. H. Trzaska[116], Y. Tsai[25], Y. Tsai[181], Z. Tsamalaidze[72], K. Tsang[181], N. Tsverava[72], S. Tufanli[36], C. Tull[125], E. Tyley[180], M. Tzanov[129], L. Uboldi[36], M. A. Uchida[30], J. Urheim[91], T. Usher[181], S. Uzunyan[148], M. R. Vagins[118], P. Vahle[208], S. Valder[189], G. A. Valdiviesso[62], E. Valencia[77], R. Valentim[198], Z. Vallari[29], E. Vallazza[97], J. W. Valle[85], S. Vallecorsa[36], R. Van Berg[163], R. G. Van de Water[128], D. Vanegas Forero[136], D. Vannerom[134], F. Varanini[100], D. Vargas[84], G. Varner[80], J. Vasel[91], S. Vasina[115], G. Vasseur[35], N. Vaughan[153], K. Vaziri[67], S. Ventura[100], A. Verdugo[40], S. Vergani[30], M. A. Vermeulen[146], M. Verzocchi[67], M. Vicenzi[71,95], H. Vieira de Souza[160], C. Vignoli[75], C. Vilela[36], B. Viren[21], T. Vrba[50], T. Wachala[145], A. V. Waldron[88], M. Wallbank[41], C. Wallis[45], H. Wang[26], J. Wang[183], L. Wang[125], M. H. Wang[67], X. Wang[67], Y. Wang[26], Y. Wang[186], K. Warburton[107], D. Warner[45], M. Wascko[88], D. Waters[200], A. Watson[17], K. Wawrowska[176,189], P. Weatherly[55], A. Weber[67,132], M. Weber[15], H. Wei[21], A. Weinstein[107], D. Wenman[209], M. Wetstein[107], A. White[194], L. H. Whitehead[30], D. Whittington[190], M. J. Wilking[186], A. Wilkinson[200], C. Wilkinson[125], Z. Williams[194], F. Wilson[176], R. J. Wilson[45], W. Wisniewski[181], J. Wolcott[197], T. Wongjirad[197], A. Wood[81], K. Wood[125], E. Worcester[21], M. Worcester[21], K. Wresilo[30], C. Wret[173], W. Wu[67], W. Wu[25], Y. Xiao[25], F. Xie[189], B. Yaeggy[41], E. Yandel[28], G. Yang[186], K. Yang[155], T. Yang[67,a], A. Yankelevich[25], N. Yershov[104], K. Yonehara[67], Y. Yoon[39], T. Young[147], B. Yu[21], H. Yu[21], H. Yu[187], J. Yu[194], Y. Yu[87], W. Yuan[58], R. Zaki[212], J. Zalesak[49], L. Zambelli[53], B. Zamorano[73], A. Zani[98], L. Zazueta[208], G. Zeller[67], J. Zennamo[67], K. Zeug[209], C. Zhang[21], S. Zhang[91], Y. Zhang[167], M. Zhao[21], E. Zhivun[21], G. Zhu[152], E. D. Zimmerman[44], S. Zucchelli[18,92], J. Zuklin[49], V. Zutshi[148], R. Zwaska[67]

[1] Abilenexs Christian University, Abilene, TX 79601, USA
[2] University of Albany, SUNY, Albany, NY 12222, USA
[3] University of Amsterdam, 1098 XG Amsterdam, The Netherlands
[4] Antalya Bilim University, Döşemealtı/Antalya 07190, Turkey
[5] University of Antananarivo, Antananarivo 101, Madagascar
[6] Universidad Antonio Nariño, Bogotá, Colombia
[7] Argonne National Laboratory, Argonne, IL 60439, USA
[8] University of Arizona, Tucson, AZ 85721, USA
[9] Universidad Nacional de Asunción, San Lorenzo, Paraguay
[10] University of Athens, Zografou 157 84, Greece
[11] Universidad del Atlántico, Barranquilla, Atlántico, Colombia
[12] Augustana University, Sioux Falls, SD 57197, USA
[13] Banaras Hindu University, Varanasi 221 005, India
[14] University of Basel, 4056 Basel, Switzerland
[15] University of Bern, 3012 Bern, Switzerland
[16] Beykent University, Istanbul, Turkey
[17] University of Birmingham, Birmingham B15 2TT, UK
[18] Università del Bologna, 40127 Bologna, Italy
[19] Boston University, Boston, MA 02215, USA
[20] University of Bristol, Bristol BS8 1TL, UK
[21] Brookhaven National Laboratory, Upton, NY 11973, USA
[22] University of Bucharest, Bucharest, Romania
[23] University of California Berkeley, Berkeley, CA 94720, USA
[24] University of California Davis, Davis, CA 95616, USA
[25] University of California Irvine, Irvine, CA 92697, USA
[26] University of California Los Angeles, Los Angeles, CA 90095, USA
[27] University of California Riverside, Riverside, CA 92521, USA
[28] University of California Santa Barbara, Santa Barbara, CA 93106, USA
[29] California Institute of Technology, Pasadena, CA 91125, USA
[30] University of Cambridge, Cambridge CB3 0HE, UK
[31] Universidade Estadual de Campinas, Campinas, SP 13083-970, Brazil
[32] Università di Catania, 2, 95131 Catania, Italy
[33] Universidad Católica del Norte, Antofagasta, Chile
[34] Centro Brasileiro de Pesquisas Físicas, Rio de Janeiro, RJ 22290-180, Brazil
[35] IRFU, CEA, Université Paris-Saclay, 91191 Gif-sur-Yvette, France
[36] CERN, The European Organization for Nuclear Research, 1211 Meyrin, Switzerland
[37] Institute of Particle and Nuclear Physics of the Faculty of Mathematics and Physics of the Charles University, 180 00, Prague 8, Czech Republic
[38] University of Chicago, Chicago, IL 60637, USA
[39] Chung-Ang University, Seoul 06974, South Korea

[40] CIEMAT, Centro de Investigaciones Energéticas, Medioambientales y Tecnológicas, 28040 Madrid, Spain
[41] University of Cincinnati, Cincinnati, OH 45221, USA
[42] Centro de Investigación y de Estudios Avanzados del Instituto Politécnico Nacional (Cinvestav), Mexico City, Mexico
[43] Universidad de Colima, Colima, Mexico
[44] University of Colorado Boulder, Boulder, CO 80309, USA
[45] Colorado State University, Fort Collins, CO 80523, USA
[46] Columbia University, New York, NY 10027, USA
[47] Centro de Tecnologia da Informacao Renato Archer, Amarais, Campinas, SP CEP 13069-901, Brazil
[48] Central University of South Bihar, Gaya 824236, India
[49] Institute of Physics, Czech Academy of Sciences, 182 00, Prague 8, Czech Republic
[50] Czech Technical University, 115 19, Prague 1, Czech Republic
[51] Dakota State University, Madison, SD 57042, USA
[52] University of Dallas, Irving, TX 75062-4736, USA
[53] Laboratoire d'Annecy de Physique des Particules, Univ. Grenoble Alpes, Univ. Savoie Mont Blanc, CNRS, LAPP-IN2P3, 74000 Annecy, France
[54] Daresbury Laboratory, Cheshire WA4 4AD, UK
[55] Drexel University, Philadelphia, PA 19104, USA
[56] Duke University, Durham, NC 27708, USA
[57] Durham University, Durham DH1 3LE, UK
[58] University of Edinburgh, Edinburgh EH8 9YL, UK
[59] Universidad EIA, Envigado, Antioquia, Colombia
[60] ETH Zurich, Zurich, Switzerland
[61] Faculdade de Ciências da Universidade de Lisboa-FCUL, 1749-016 Lisbon, Portugal
[62] Universidade Federal de Alfenas, Poços de Caldas, MG 37715-400, Brazil
[63] Universidade Federal de Goias, Goiania, GO 74690-900, Brazil
[64] Universidade Federal de São Carlos, Araras, SP 13604-900, Brazil
[65] Universidade Federal do ABC, Santo André, SP 09210-580, Brazil
[66] Universidade Federal do Rio de Janeiro, Rio de Janeiro, RJ 21941-901, Brazil
[67] Fermi National Accelerator Laboratory, Batavia, IL 60510, USA
[68] University of Ferrara, Ferrara, Italy
[69] University of Florida, Gainesville, FL 32611-8440, USA
[70] Fluminense Federal University, 9 Icaraí, Niterói, RJ 24220-900, Brazil
[71] Università degli Studi di Genova, Genoa, Italy
[72] Georgian Technical University, Tbilisi, Georgia
[73] University of Granada and CAFPE, 18002 Granada, Spain
[74] Gran Sasso Science Institute, L'Aquila, Italy
[75] Laboratori Nazionali del Gran Sasso, L'Aquila, AQ, Italy
[76] University Grenoble Alpes, CNRS, Grenoble INP, LPSC-IN2P3, 38000 Grenoble, France
[77] Universidad de Guanajuato, Guanajuato C.P. 37000, Mexico
[78] Harish-Chandra Research Institute, Jhunsi, Allahabad 211 019, India
[79] Harvard University, Cambridge, MA 02138, USA
[80] University of Hawaii, Honolulu, HI 96822, USA
[81] University of Houston, Houston, TX 77204, USA
[82] University of Hyderabad, Gachibowli, Hyderabad 500 046, India
[83] Idaho State University, Pocatello, ID 83209, USA
[84] Institut de Física d'Altes Energies (IFAE)-Barcelona Institute of Science and Technology (BIST), Barcelona, Spain
[85] Instituto de Física Corpuscular, CSIC and Universitat de València, 46980 Paterna, Valencia, Spain
[86] Instituto Galego de Fisica de Altas Enerxias, A Coruña, Spain
[87] Illinois Institute of Technology, Chicago, IL 60616, USA
[88] Imperial College of Science Technology and Medicine, London SW7 2BZ, UK
[89] Indian Institute of Technology Guwahati, Guwahati 781 039, India
[90] Indian Institute of Technology Hyderabad, Hyderabad 502285, India
[91] Indiana University, Bloomington, IN 47405, USA
[92] Istituto Nazionale di Fisica Nucleare Sezione di Bologna, 40127 Bologna, Italy
[93] Istituto Nazionale di Fisica Nucleare Sezione di Catania, 95123 Catania, Italy
[94] Istituto Nazionale di Fisica Nucleare Sezione di Ferrara, 44122 Ferrara, Italy
[95] Istituto Nazionale di Fisica Nucleare Sezione di Genova, 16146 Genoa, Italy
[96] Istituto Nazionale di Fisica Nucleare Sezione di Lecce, 73100 Lecce, Italy
[97] Istituto Nazionale di Fisica Nucleare Sezione di Milano Bicocca, 3, 20126 Milan, Italy
[98] Istituto Nazionale di Fisica Nucleare Sezione di Milano, 20133 Milan, Italy
[99] Istituto Nazionale di Fisica Nucleare Sezione di Napoli, 80126 Naples, Italy
[100] Istituto Nazionale di Fisica Nucleare Sezione di Padova, 35131 Padua, Italy
[101] Istituto Nazionale di Fisica Nucleare Sezione di Pavia, 27100 Pavia, Italy
[102] Istituto Nazionale di Fisica Nucleare Laboratori Nazionali del Sud, 95123 Catania, Italy
[103] Universidad Nacional de Ingeniería, Lima 25, Peru
[104] Institute for Nuclear Research of the Russian Academy of Sciences, Moscow 117312, Russia

[105] University of Insubria, Via Ravasi 2, 21100 Varese, Italy
[106] University of Iowa, Iowa City, IA 52242, USA
[107] Iowa State University, Ames, IA 50011, USA
[108] Institut de Physique des 2 Infinis de Lyon, 69622 Villeurbanne, France
[109] Institute for Research in Fundamental Sciences, Tehran, Iran
[110] Instituto Superior Técnico-IST, Universidade de Lisboa, 1049-001 Lisbon, Portugal
[111] Iwate University, Morioka, Iwate 020-8551, Japan
[112] University of Jammu, Jammu 180006, India
[113] Jawaharlal Nehru University, New Delhi 110067, India
[114] Jeonbuk National University, Jeonrabuk-do 54896, South Korea
[115] Joint Institute for Nuclear Research, Dzhelepov Laboratory of Nuclear Problems, 6 Joliot-Curie, Dubna, Moscow Region 141980, Russia
[116] University of Jyvaskyla, 40014 Jyvaskyla, Finland
[117] Kansas State University, Manhattan, KS 66506, USA
[118] Kavli Institute for the Physics and Mathematics of the Universe, Kashiwa, Chiba 277-8583, Japan
[119] High Energy Accelerator Research Organization (KEK), Ibaraki 305-0801, Japan
[120] Korea Institute of Science and Technology Information, Daejeon 34141, South Korea
[121] K L University, Vaddeswaram, Andhra Pradesh 522502, India
[122] National Institute of Technology, Kure College, Hiroshima 737-8506, Japan
[123] Taras Shevchenko National University of Kyiv, 01601 Kyiv, Ukraine
[124] Lancaster University, Lancaster LA1 4YB, UK
[125] Lawrence Berkeley National Laboratory, Berkeley, CA 94720, USA
[126] Laboratório de Instrumentação e Física Experimental de Partículas, 1649-003 Lisboa and 3004-516 Coimbra, Portugal
[127] University of Liverpool, L69 7ZE Liverpool, UK
[128] Los Alamos National Laboratory, Los Alamos, NM 87545, USA
[129] Louisiana State University, Baton Rouge, LA 70803, USA
[130] University of Lucknow, Lucknow, Uttar Pradesh 226007, India
[131] Madrid Autonoma University and IFT UAM/CSIC, 28049 Madrid, Spain
[132] Johannes Gutenberg-Universität Mainz, 55122 Mainz, Germany
[133] University of Manchester, Manchester M13 9PL, UK
[134] Massachusetts Institute of Technology, Cambridge, MA 02139, USA
[135] Max-Planck-Institut, 80805 Munich, Germany
[136] University of Medellín, Medellín 050026, Colombia
[137] University of Michigan, Ann Arbor, MI 48109, USA
[138] Michigan State University, East Lansing, MI 48824, USA
[139] Università del Milano-Bicocca, 20126 Milan, Italy
[140] Università degli Studi di Milano, 20133 Milan, Italy
[141] University of Minnesota Duluth, Duluth, MN 55812, USA
[142] University of Minnesota Twin Cities, Minneapolis, MN 55455, USA
[143] University of Mississippi University, University, MS 38677, USA
[144] University of New Mexico, Albuquerque, NM 87131, USA
[145] H. Niewodniczański Institute of Nuclear Physics, Polish Academy of Sciences, Cracow, Poland
[146] Nikhef National Institute of Subatomic Physics, 1098 XG Amsterdam, The Netherlands
[147] University of North Dakota, Grand Forks, ND 58202-8357, USA
[148] Northern Illinois University, DeKalb, IL 60115, USA
[149] Northwestern University, Evanston, IL 60208, USA
[150] University of Notre Dame, Notre Dame, IN 46556, USA
[151] Occidental College, Los Angeles, CA 90041, USA
[152] Ohio State University, Columbus, OH 43210, USA
[153] Oregon State University, Corvallis, OR 97331, USA
[154] National Centre for Nuclear Research, A. Soltana 7, 05 400 Otwock, Poland
[155] University of Oxford, Oxford OX1 3RH, UK
[156] Pacific Northwest National Laboratory, Richland, WA 99352, USA
[157] Universtà degli Studi di Padova, 35131 Padua, Italy
[158] Panjab University, Chandigarh, UT 160014, India
[159] Université Paris-Saclay, CNRS/IN2P3, IJCLab, 91405 Orsay, France
[160] Université de Paris, CNRS, Astroparticule et Cosmologie, 75006 Paris, France
[161] Università degli Studi di Parma, 43121 Parma, Italy
[162] Università degli Studi di Pavia, 27100 Pavia, Italy
[163] University of Pennsylvania, Philadelphia, PA 19104, USA
[164] Pennsylvania State University, University Park, PA 16802, USA
[165] Physical Research Laboratory, Ahmedabad 380 009, India
[166] Università di Pisa, 56127 Pisa, Italy
[167] University of Pittsburgh, Pittsburgh, PA 15260, USA
[168] Pontificia Universidad Católica del Perú, Lima, Peru
[169] University of Puerto Rico, Mayaguez, PR 00681, USA
[170] Punjab Agricultural University, Ludhiana 141004, India

[171] Queen Mary University of London, London, E1 4NS, UK
[172] Radboud University, 6525 AJ Nijmegen, The Netherlands
[173] University of Rochester, Rochester, NY 14627, USA
[174] Royal Holloway College, London TW20 0EX, UK
[175] Rutgers University, Piscataway, NJ 08854, USA
[176] STFC Rutherford Appleton Laboratory, Didcot OX11 0QX, UK
[177] Università del Salento, 73100 Lecce, Italy
[178] San Jose State University, San José, CA 95192-0106, USA
[179] Universidad Sergio Arboleda, 11022 Bogotá, Colombia
[180] University of Sheffield, Sheffield S3 7RH, UK
[181] SLAC National Accelerator Laboratory, Menlo Park, CA 94025, USA
[182] University of South Carolina, Columbia, SC 29208, USA
[183] South Dakota School of Mines and Technology, Rapid City, SD 57701, USA
[184] South Dakota State University, Brookings, SD 57007, USA
[185] Southern Methodist University, Dallas, TX 75275, USA
[186] Stony Brook University, SUNY, Stony Brook, NY 11794, USA
[187] Sun Yat-Sen University, Guangzhou 510275, China
[188] Sanford Underground Research Facility, Lead, SD 57754, USA
[189] University of Sussex, Brighton BN1 9RH, UK
[190] Syracuse University, Syracuse, NY 13244, USA
[191] Universidade Tecnológica Federal do Paraná, Curitiba, Brazil
[192] Texas A&M University, College Station, TX 77840, USA
[193] Texas A&M University-Corpus Christi, Corpus Christi, TX 78412, USA
[194] University of Texas at Arlington, Arlington, TX 76019, USA
[195] University of Texas at Austin, Austin, TX 78712, USA
[196] University of Toronto, Toronto, ON M5S 1A1, Canada
[197] Tufts University, Medford, MA 02155, USA
[198] Universidade Federal de São Paulo, São Paulo 09913-030, Brazil
[199] Ulsan National Institute of Science and Technology, Ulsan 689-798, South Korea
[200] University College London, London WC1E 6BT, UK
[201] Valley City State University, Valley City, ND 58072, USA
[202] Variable Energy Cyclotron Centre, Kolkata, West Bengal 700 064, India
[203] Virginia Tech, Blacksburg, VA 24060, USA
[204] University of Warsaw, 02-093 Warsaw, Poland
[205] University of Warwick, Coventry CV4 7AL, UK
[206] Wellesley College, Wellesley, MA 02481, USA
[207] Wichita State University, Wichita, KS 67260, USA
[208] College of William and Mary, Williamsburg, VA 23187, USA
[209] University of Wisconsin Madison, Madison, WI 53706, USA
[210] Yale University, New Haven, CT 06520, USA
[211] Yerevan Institute for Theoretical Physics and Modeling, Yerevan 0036, Armenia
[212] York University, Toronto M3J 1P3, Canada

Received: 31 March 2022 / Accepted: 12 September 2022

Abstract Liquid argon time projection chamber detector technology provides high spatial and calorimetric resolutions on the charged particles traversing liquid argon. As a result, the technology has been used in a number of recent neutrino experiments, and is the technology of choice for the Deep Underground Neutrino Experiment (DUNE). In order to perform high precision measurements of neutrinos in the detector, final state particles need to be effectively identified, and their energy accurately reconstructed. This article proposes an algorithm based on a convolutional neural network to perform the classification of energy deposits and reconstructed particles as track-like or arising from electromagnetic cascades. Results from testing the algorithm on experimental data from ProtoDUNE-SP, a prototype of the DUNE far detector, are presented. The network identifies track- and shower-like particles, as well as Michel electrons, with high efficiency. The performance of the algorithm is consistent between experimental data and simulation.

1 Introduction

The ProtoDUNE single phase detector (ProtoDUNE-SP) [1,2] is a prototype liquid argon time projection chamber (LArTPC) for the Deep Underground Neutrino Experiment (DUNE) far detector [3,4]. ProtoDUNE-SP is known as a

---

[a] e-mail: tjyang@fnal.gov (corresponding author)

single phase detector as it is operated entirely within liquid phase argon. The detector readout mechanism consists of six Anode Plane Assemblies (APAs), each containing three wire readout planes at angles of ± 36° and 0° to the vertical, where the readout planes are denoted U, V and W, respectively. The U and V views are the induction views, meaning that charge is induced on the wires by drifting electrons, and the W-view wires collect the drifting electrons. The wires in each readout plane are spaced with approximately 5 mm pitch and are read out at a rate of 2 MHz. A full description of the detector is given in Ref. [2]. ProtoDUNE-SP collected data from a positively-charged-particle beam at CERN [5,6] in autumn 2018, including charged pions, charged kaons, protons, muons and positrons recorded with momenta in the range from 0.3 to 7 GeV/c. Additionally, since ProtoDUNE-SP is located on the Earth's surface, it is subject to a large flux of cosmic ray muons.

The particle interactions can be easily and naturally visualised as three two-dimensional images (one for each readout view) in the wire number and time parameter space. Each pixel in the image represents the measured charge from a reconstructed energy deposition, called a *hit*, on a given wire at a given time. A major challenge in the automated reconstruction of particle interactions in LArTPCs is identifying whether energy deposits originate from track-like (linear, such as protons, charged kaons, charged pions, and muons) or shower-like (locally dense, such as electrons and photons) structures. An example of a 7 GeV/c charged pion interaction is given in Fig. 1, where the π^+ enters the detector and interacts (just after wire 200 and at time tick 4500) producing a number of track- and shower-like particles. In order to classify the interaction type of the π^+, for example as charge-exchange or inelastic scattering, the particles emitted from the interaction vertex must be identified. The classification of reconstructed particles as track-like or shower-like will also be important in DUNE for the correct classification of neutrino interactions in the far detector. The identification of Michel electrons helps to distinguish between μ^+ and μ^-. It can also be used to identify stopping charged pions whose energy can be fully reconstructed.

In this article, we propose and demonstrate the use of a convolutional neural network (CNN) to classify hits as either belonging to track-like or shower-like structures [7]. Furthermore, a Michel electron score is given to each hit to help identify Michel electrons and positrons, produced in the decay of muons and antimuons, respectively [8].[1] These hit-level classifications can be used alongside pattern recognition based reconstruction algorithms such as Pandora [9,10] to refine the track or shower classification of reconstructed particles. The performance of the Pandora reconstruction on ProtoDUNE-SP simulated and experimental data is described in detail in Ref. [11]. Convolutional neural networks have been successfully used in neutrino physics for event classification [12–14], particle identification [15,16] and reconstruction [17]. The fine-grain images obtained from LArTPC detectors makes CNNs a natural choice for such tasks. This algorithm is novel in that it aims to classify the hits based on a small local neighbourhood as opposed to a semantic segmentation approach that uses a much larger image containing a large part (or all) of the detector. The algorithm was designed in this way to minimise the memory usage and computational processing time, allowing it to run quickly on standard computing node CPUs where there is no access to powerful GPUs.

2 The convolutional neural network

Convolutional neural networks extract features from images by applying a series of filters that are learned during the training process [18,19]. The number of filters and the number of convolutional layers varies for each specific use case; they are determined by the class of problem the network is trying to solve, and the computer hardware available for training and evaluating the network. In this case, a GPU was available for the training of the network, but the inference is performed on computing cluster CPUs (where GPUs are typically not available) as a part of the ProtoDUNE-SP reconstruction chain. As a result, only simple architectures containing few convolutional layers were considered, constrained by the desired evaluation time on the CPUs. For inference tasks within the ProtoDUNE-SP event reconstruction workflow, a C++ interface was added to the LArSoft framework [20]. Recent attempts to introduce GPU acceleration into the workflow mentioned above show promising reductions in processing time [21].

The input to the network is a small region of the entire detector image known as a *patch*. For each reconstructed hit object, the wire number w and peak time t are extracted, and a 48 × 48 pixel image, centred on (w, t), is created and the value of each pixel corresponds to the detected charge on a given wire at a given time. The wire dimension of the image corresponds to 48 wires with one wire per pixel. The time data are downsampled by averaging over six time samples, such that the spatial dimensions of the pixels match the 5 mm wire pitch in both directions. Therefore, each image represents around 24×24 cm^2 of wire data. Figure 2 shows the hits from one APA in a simulated ProtoDUNE-SP event and the three zoomed regions give example 48 × 48 pixel patches in the track, shower and Michel categories. Detector effects such as the ones introduced by space charge [1,22] are included in the simulation. The images from the three wire planes are independently evaluated. This paper only reports on results

---

[1] Michel electron will be used to refer to both Michel electrons and Michel positrons.

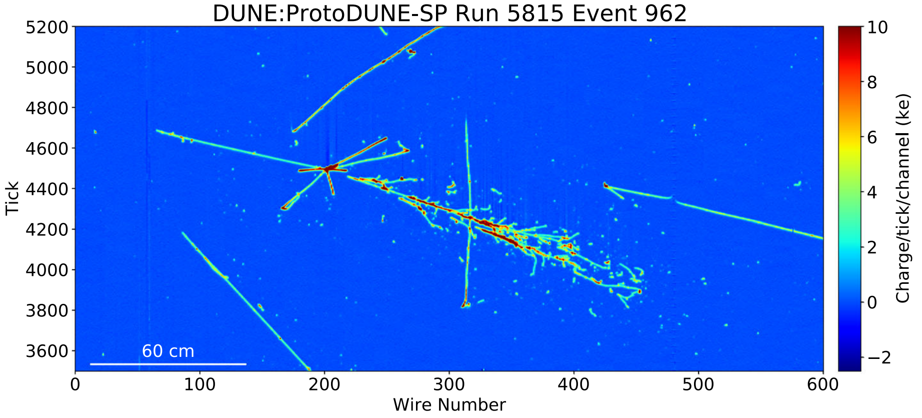

Fig. 1 A 7 GeV/c beam π^+ interaction in the collection view (W-view) in ProtoDUNE-SP data. The x axis shows the wire number. The y axis shows the time tick in the unit of 0.5 µs. The colour scale represents the charge deposition

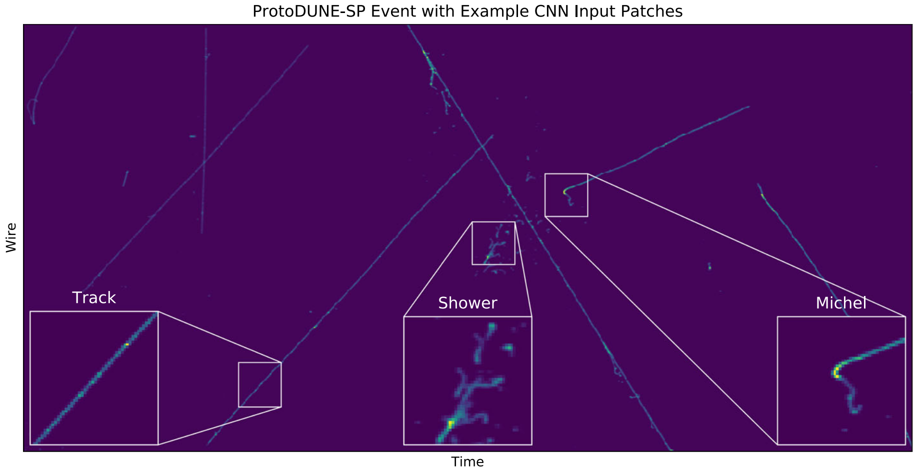

Fig. 2 Examples of CNN input patches from a simulated ProtoDUNE-SP event. The inputs to the CNN are small 48 × 48 pixel images created from patches of the full detector readout. Three examples are shown, each labelled with their appropriate class. The patch of the detector readout from which each patch was generated is emphasised

from the collection plane, which has the highest signal-to-noise ratio.

The architecture for this hit-tagging CNN is shown in Fig. 3. A single convolutional layer containing 48 5 × 5 pixel filters is used to extract feature maps from the input image, which are then flattened and passed to two dense layers that use them to classify the images. Two dropout[2] layers are used for regularisation [23]. The output of the network is split into two branches. The first branch returns the scores for track, shower, or empty (TSE) classification, which can be interpreted as probabilities as they are constrained to sum to one by a softmax [24] activation function. The second returns the probability for a Michel electron classification, with a sigmoid [24] activation function. The output of the network is split in this way due to the overlap of the shower and Michel electron classes. The total loss function is a weighted sum of the two branches, with the weights derived from the relative size of the training samples in each branch.

2.1 Training details

For the purposes of training a true classification must be attached to each of the patches. In addition to track, shower and Michel electron patches, empty patches are also created where the central pixel contains no energy deposit. Approximately 30 million images were prepared in total using approximately 500 simulated events: ∼ 15 million in the track sample, ∼ 11 million in the shower sample, ∼ 3 million in the empty sample, and ∼ 1 million in the Michel electron sample.

The CNN was trained with TensorFlow [25] through its Keras [26] interface, and performance metrics, such as the losses, purity and efficiency, were monitored throughout training using TensorBoard [27]. Before training, the data set was split into training, test, and validation sets in the ratio 80:10:10. The performance metrics were monitored throughout training with the training and validation sets, and again after training with the test set. Figure 4 shows the evolution of the training and validation losses throughout the training. Due to the large number of training images and relative simplicity of the task, the losses fall sharply within the first epoch, which is not visible in the plots. The training and validation losses begin to diverge after the first few epochs suggesting

---

[2] Dropout randomly disables a given fraction of neurons for each training example.

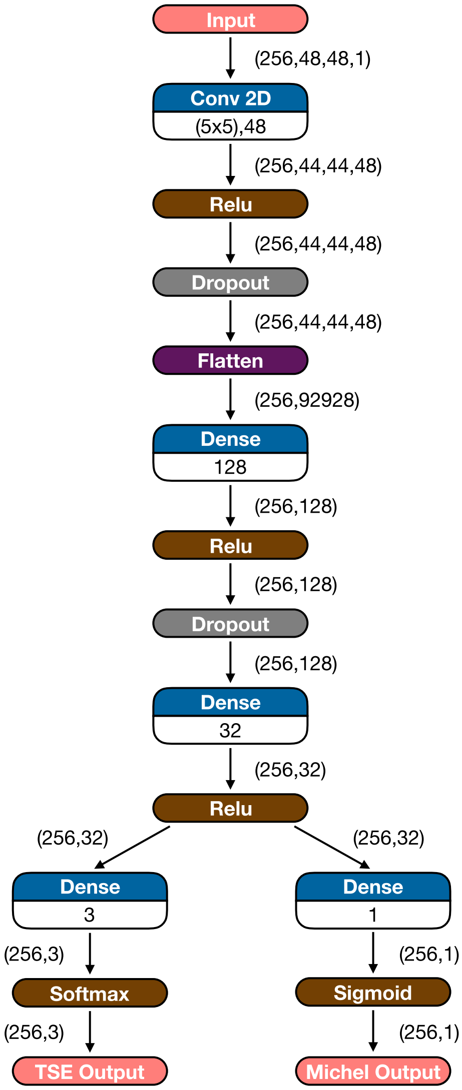

Fig. 3 The CNN architecture. In this case, the CNN processes 256 images in parallel. Each image is a 48 × 48 pixel patch of the calibrated detector readout. A single convolutional layer, with 48 filters of size 5 × 5, is used to extract features from the images. These are processed by two dense layers containing 128 and 32 neurons respectively, before being split into two branches which provide the track-shower-empty (TSE) and Michel outputs. The dimensions of the data after each operation are given next to the black arrows

there is some over-fitting, but the network generalises well when considering the similar performance of the algorithm on the test and validation sets. To further ensure generalisation, an early stopping algorithm was used, which focused on the loss in the TSE branch [28]. The final weights for the network were taken from a checkpoint at the end of the fifth epoch[3] since the validation loss in the TSE branch starts to plateau on the fifth epoch.

2.2 Performance

The performance of the hit tagging was evaluated with reconstructed events from ProtoDUNE-SP simulation. A 48 × 48 pixel image is created around each reconstructed hit, which is then classified by the network and the classification compared with the truth label. Note that by definition this method ensures that no processing is performed on empty images. Figure 5 shows the shower score distributions for true shower hits and all other hits, and a strong separation is seen between the distributions with a score close to one corresponding to a hit that is highly likely to come from a shower. The small peak in the *other hits* distribution close to one comes from delta-ray electrons overlapping with the cosmic-ray muon that produced them. The classification threshold can be set on a case by case basis, for the initial validation of the network on the ProtoDUNE-SP data it was optimised based on the F1 score, which is given by:

$$\frac{1}{F_1} = \frac{1}{2}\left(\frac{1}{\text{purity}} + \frac{1}{\text{efficiency}}\right), \tag{1}$$

where the purity is defined as the fraction of correctly classified shower hits in the sample of all selected shower hits, and the efficiency as the fraction of all true shower hits that were selected as shower hits.

Figure 6 demonstrates the performance of the network in terms of the true positive and false positive rates. In this case, the true positive rate is the fraction of true shower hits that have been correctly classified as shower hits, and the false positive rate is the fraction of other hits incorrectly classified as shower hits. The receiver operating characteristic (ROC) curve is shown, which shows the true positive rate against the false positive rate as the selection threshold on the shower classifier output is varied. ROC curves are shown for simulation with the space charge effect (SCE, red) and without (blue). The close agreement between the curves suggests that the CNN results are robust against changes in the SCE model.

The score distributions from the Michel electron classifier are shown in Fig. 7, for true Michel electron hits and all other hits. The Michel electron classification is a significantly more challenging problem, partly due to the large variation in Michel electron interactions in the detector. Michel electrons can be seen as single short track-like objects, or more fragmented due to photon emission and subsequent Compton scattering to produce additional electrons. Furthermore, some delta-ray electrons and components of electromagnetic showers can produce signatures in the detector that are similar to Michel electrons. Therefore, while both distributions are strongly peaked at the expected values, with Michel electrons close to one and other hits close to zero, there are also subleading peaks of hits that are not correctly classified. Due to this, and the significantly smaller sample of Michel electron hits, the network is not able to achieve a good performance

---

[3] An epoch is defined as one iteration over the entire training sample.

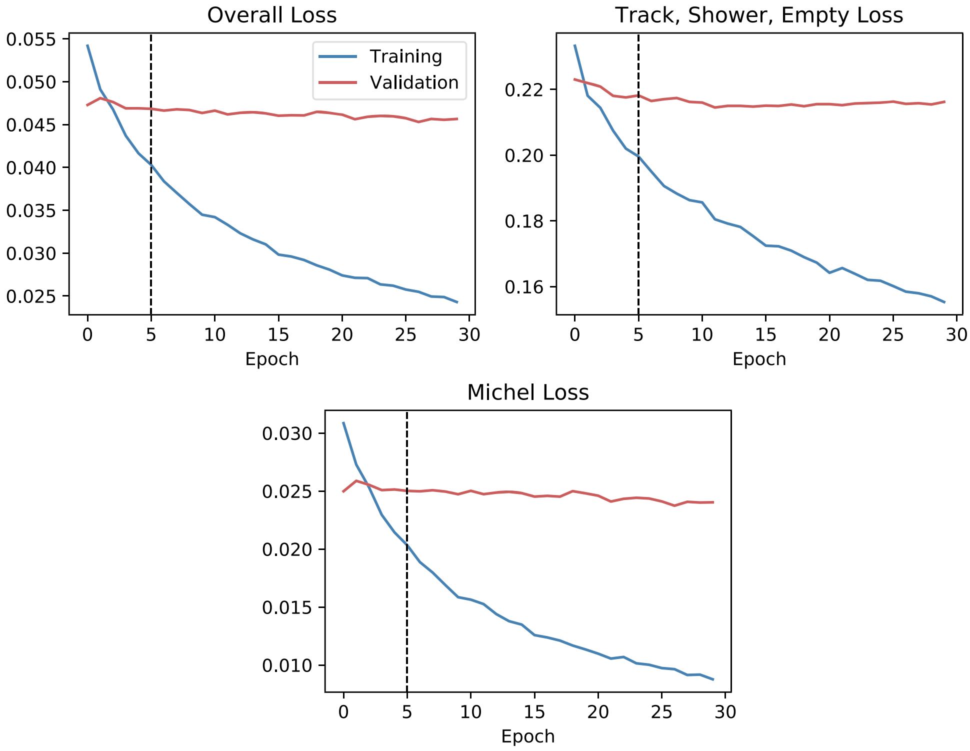

Fig. 4 Evolution of the training and validation losses as a function of training epoch. The final weights of the network were taken from a checkpoint at the end of the fifth epoch, shown here as a vertical line. The overall loss; track, shower and empty loss; and Michel loss are shown in the top left, top right, and bottom left respectively. In calculating the overall loss, the track, shower and empty loss is weighted by 0.1 to be consistent with the smaller size of the Michel sample

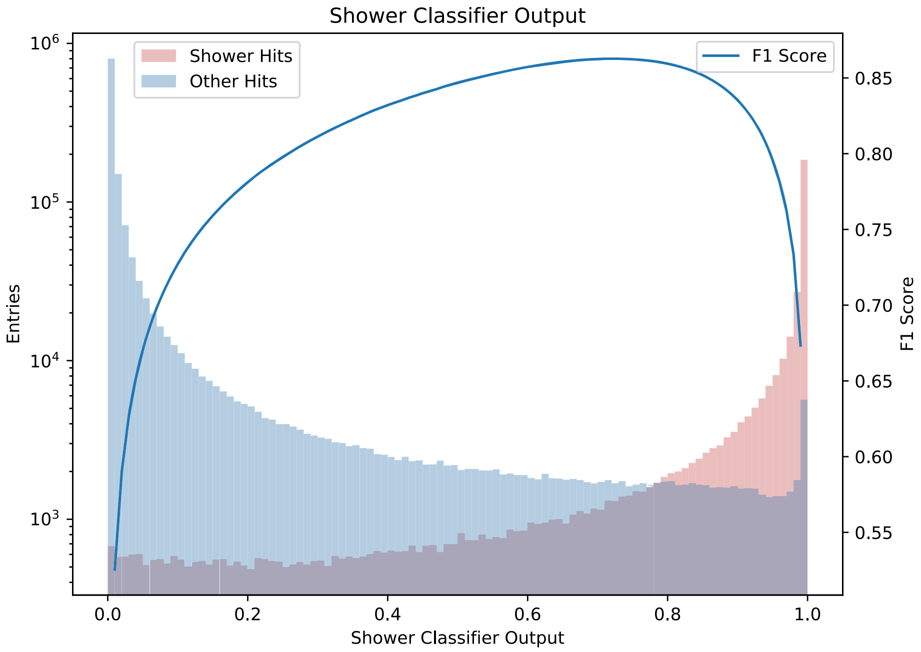

Fig. 5 Shower classifier output distributions. The output of the shower classifier is shown for true shower hits in red and all other hits in blue. The blue line shows the F1 score as a function of classification threshold

in terms of the F1 metric. However, when combined with simple clustering, a high purity sample of Michel electron events can be selected, as will be discussed in Sect. 3.

3 Results from experimental data and simulation

It is important that the CNN is robust against potential differences between experimental data and simulation, and hence the performance has been compared between experimental data and simulation for several particle species. Hits are tagged in the three different readout views and reconstructed particles from Pandora are assigned a score between 0 and 1 that is the average of the shower classifier score from the CNN from all of the 2D hits in the collection view. Each hit is weighted by the hit charge when calculating the average shower score. A score close to one means that it is highly

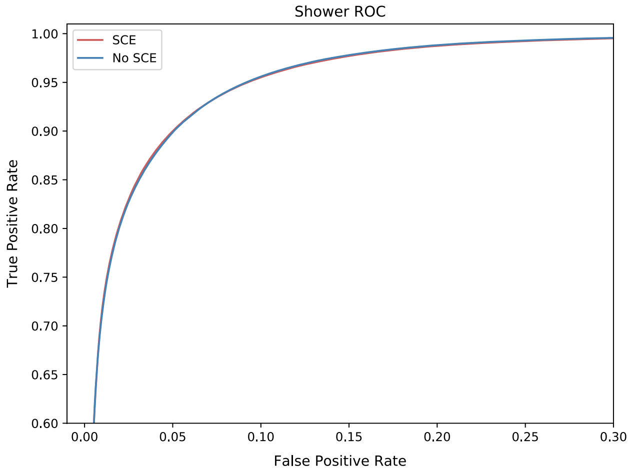

Fig. 6 ROC curves for the shower classifier, showing the true positive rate against false the positive rate for varying classification threshold on the shower classifier output. The red (blue) line shows the ROC curve from ProtoDUNE-SP simulation with (without) SCE. The red curve is obscured by the blue due to close agreement

probable that the particle is shower-like, and a low score means the particle is very likely to be track-like.

Data from ProtoDUNE-SP runs 5387 and 5809 taken in the H4-VLE test beam at CERN with 1 GeV/c beam momentum were used for the initial qualitative validation of the CNN performance on ProtoDUNE-SP data. These runs contain cosmic rays and particles from the charged particle beam. Run 5809 was taken with the inclusive beam trigger giving a dataset primarily consisting of beam positrons. Run 5387 was taken with a trigger that vetoed positrons, which resulted in a sample primarily consisting of beam π^+'s, μ^+'s and protons. Figure 8 shows an example of the CNN shower scores of reconstructed particles in a ProtoDUNE-SP event as a visual cross-check of the CNN performance. As expected, the cosmic-ray muon and pion tracks in the event have low shower scores, while the photon shower from the charged particle beam interaction is given a high score. In addition, delta ray electrons, which are emitted along the muon tracks, are associated with showers and therefore receive a high CNN shower score. The latest ProtoDUNE-SP Monte Carlo (MC) simulation sample was used to compare with experimental data. This is a new MC simulation with improved modelling of detector response, which is completely independent of the previous MC simulation that was used to train the CNN.

The following sections report the performance of the CNN classification at the hit level and the particle level for cosmic rays and charged particles from the test beam. In order to classify the hits, a threshold of 0.72 was applied to the shower classifier output of the CNN, with hits exceeding the threshold being classified as shower hits. This threshold was selected by choosing the value with the largest F1 score in Fig. 5. For particle-level classification, a different threshold of 0.81 is applied to the average shower score to classify particles, where the threshold was chosen to maximise the product of the selection efficiencies of all four types of charged beam particles.

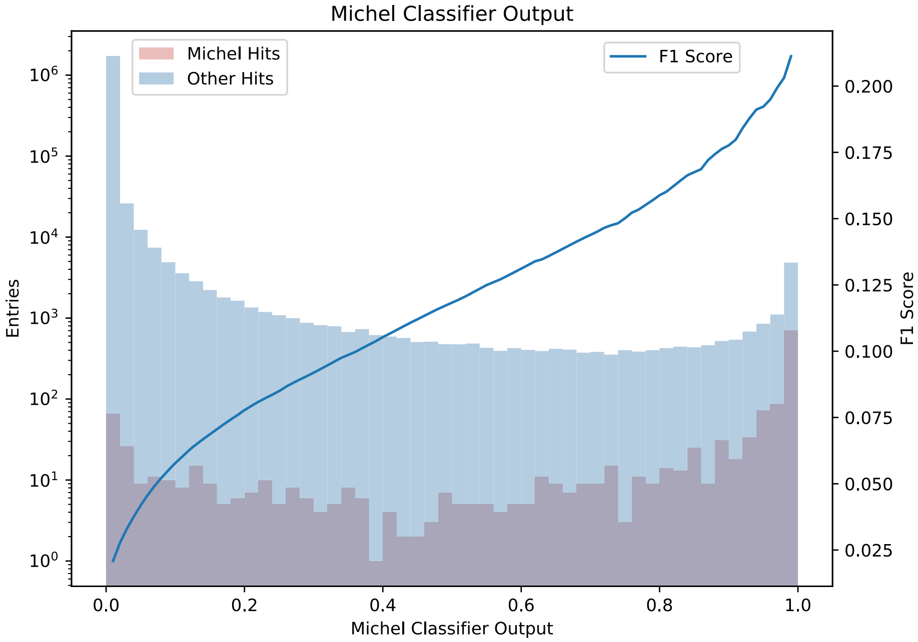

Fig. 7 Michel electron classifier output distributions

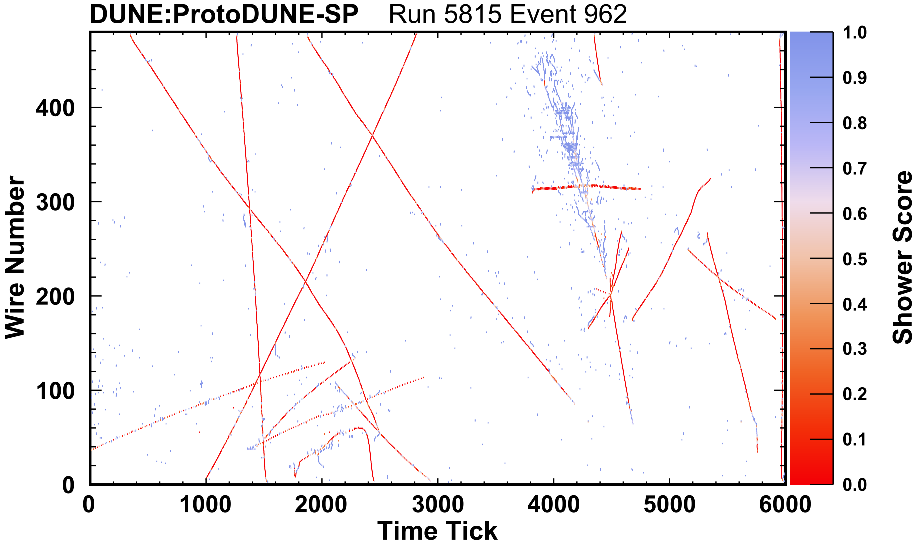

Fig. 8 The CNN shower score of each hit in reconstructed particles for the same 7 GeV/c π^+ interaction shown in Fig. 1. This diagram shows the location of reconstructed hits in wire-time coordinates, and the hits are coloured based on the CNN shower score. Red hits are track-like, and blue hits are shower-like. A number of cosmic muon tracks can be seen, along with tracks and showers produced by the pion interaction. The small shower-like patches along the muon tracks are delta-ray electrons

3.1 Cosmic-ray muons

The CNN was first tested on a sample of cosmic-ray muons[4] in order to validate its performance before it was used to classify beam particles (see Sect. 3.2). A sample of cosmic-ray muons was selected from simulation and experimental data (run 5387), where cosmic-ray muon candidates were selected using the following criteria:

- the particle was reconstructed by Pandora as a track
- the track was at least 1 m in length
- the track started and ended at least 50 cm from the front face of the detector (to veto beam particles)
- the track was directed at least 15° away from the vertical (to veto tracks that only deposited energy on a small number of collection plane wires).

All of the hits associated to the selected tracks were labelled as true cosmic-ray muon hits. The hits from any other particles associated with the cosmic-ray muon candidate, such as delta-ray and Michel electrons, were not included to avoid contaminating the hit selection.

Firstly, the hit-level classification was studied. Figure 9 shows the CNN shower output score for cosmic-ray hits in experimental data (black) and simulation (red), and demonstrates the high level of agreement between the two samples. The peak in the score distribution close to one can be attributed to hits from the numerous delta-ray electrons produced by high energy muons, such as those shown previously in Fig. 8. The results of the hit-level classification, obtained by measuring the fraction of hits below a threshold of 0.72, are given in Table 1.

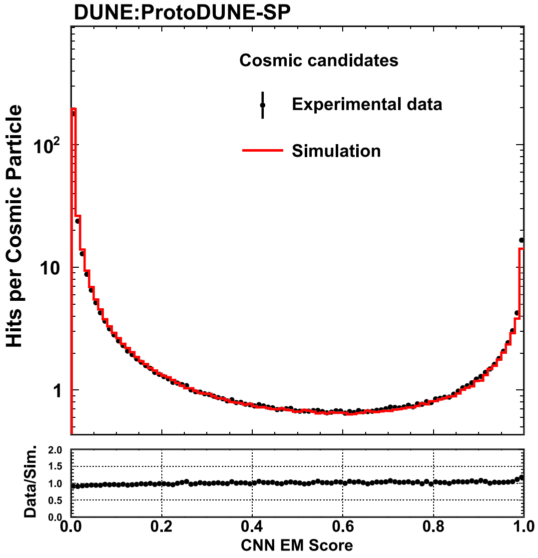

Fig. 9 The CNN shower classifier scores for cosmic-ray muon hits from experimental data (black) and simulation (red). The error bars on the data are statistical

Table 1 The fraction of correctly classified cosmic-ray muon hits and particles using the CNN measured for experimental data and simulation. The errors represent the statistical uncertainties calculated using the Clopper–Pearson method [29]

Stage	Correctly classified (%)		Data/simulation
	Data	Simulation	
Hits	85.6 ± 0.0	87.3 ± 0.0	0.980 ± 0.000
Particles	99.8 ± 0.1	$100.0^{+0.0}_{-0.1}$	0.998 ± 0.002

Figure 10 shows the particle-level comparison of the average CNN shower score for the cosmic-ray muons in experimental data and simulation. As expected, the distributions are peaked close to zero, and the experimental data distribution is

---

[4] Since ProtoDUNE-SP does not have a magnetic field this sample also contains antimuons.

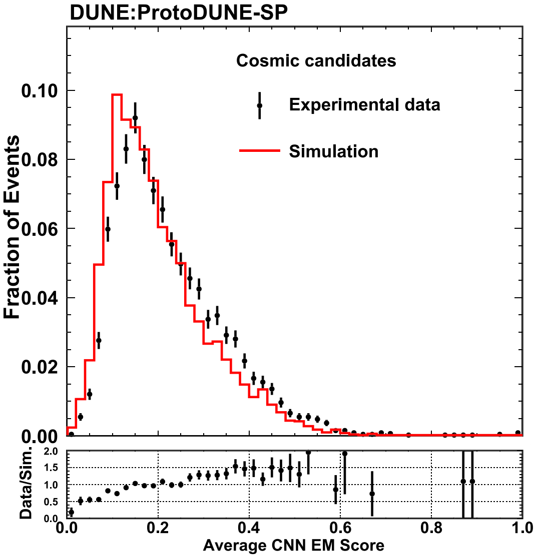

Fig. 10 The average CNN shower classifier scores for cosmic-ray muons. The error bars on the experimental data are statistical

Table 2 Numbers of events after the beam quality and number of hits selection criteria shown for experimental data and simulation

	π^+	μ^+	p	e^+
Data	5402	1228	9364	9106
Simulation	16612	1305	23660	42245
Simulation purity	84.4%	86.7%	99.8%	97.7%

slightly shifted compared to the simulation. However, when applying the threshold of 0.81 to classify the cosmic rays as track-like, both the performance and agreement between experimental data and simulation is excellent, as shown in Table 1.

3.2 Charged particle test beam

In the case of particles originating from the charged particle beam in the experimental data samples, the beam instrumentation [1] can be used to provide an effective truth source

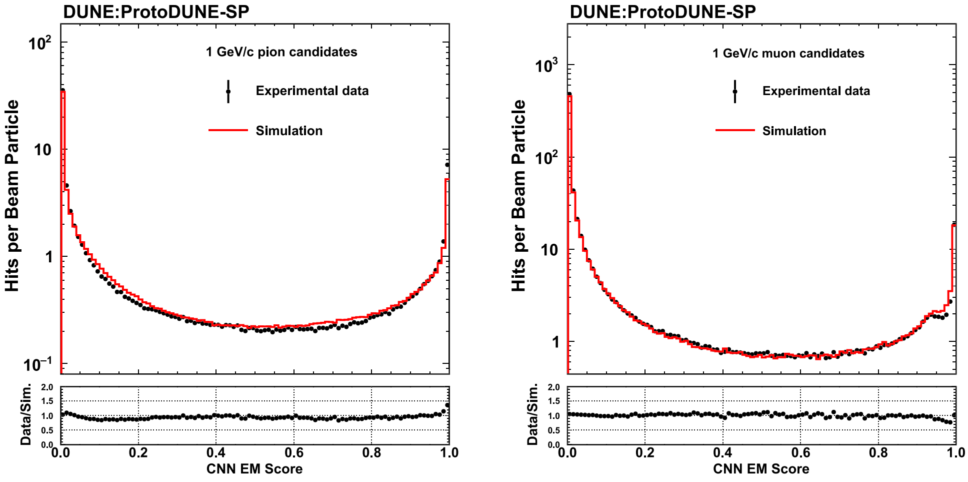

(a) pion **(b)** muon

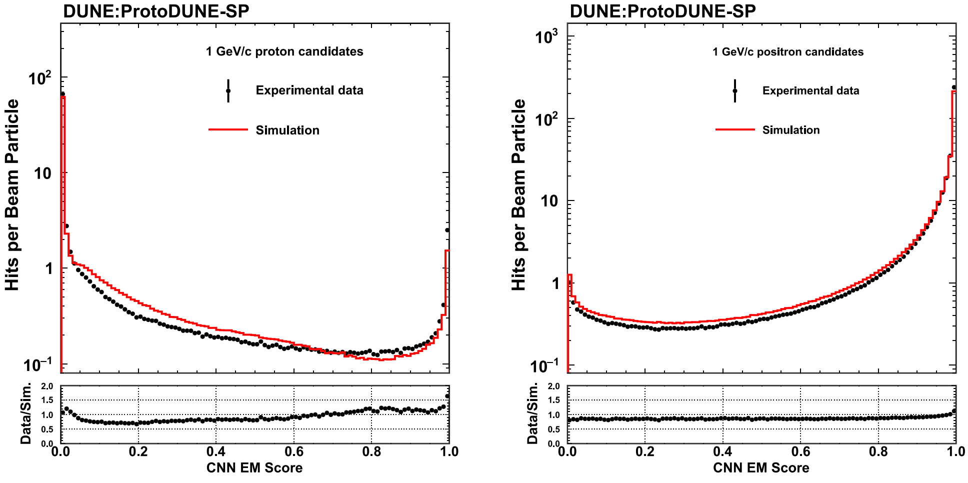

(c) proton **(d)** positron

Fig. 11 Shower classifier scores for different particle species in the ProtoDUNE-SP beam. The error bars on the experimental data are statistical

Table 3 Fraction of hits classified into appropriate class for different samples in ProtoDUNE-SP data and simulation. The statistical uncertainties on the fractions and ratios are negligible

Hit Source	Class	Data fraction (%)	Simulation fraction (%)	Data/simulation
Pion	Track	78.7	80.3	0.98
Muon	Track	92.7	92.0	1.01
Proton	Track	93.0	94.5	0.98
Positron	Shower	93.0	91.4	1.02

Fig. 12 Average shower classifier scores for different particle species in the ProtoDUNE-SP beam. The error bars on the experimental data are statistical

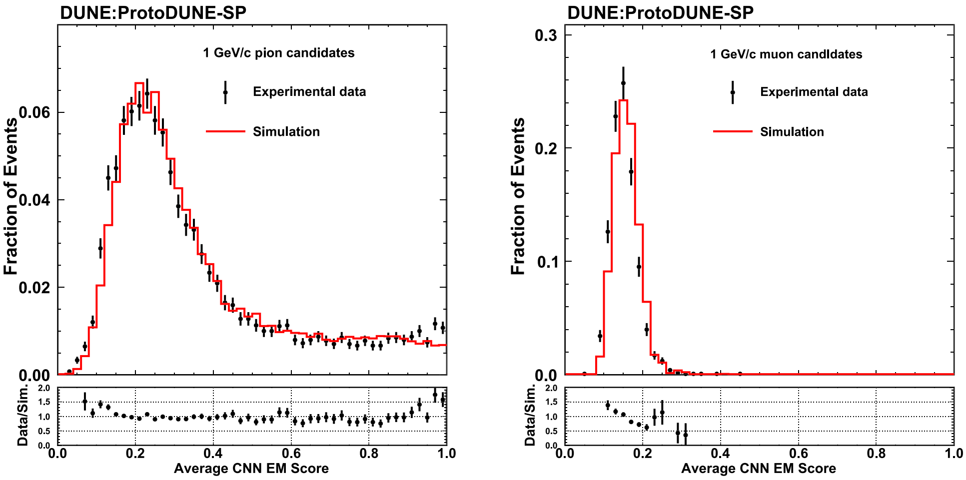

(a) pion **(b)** muon

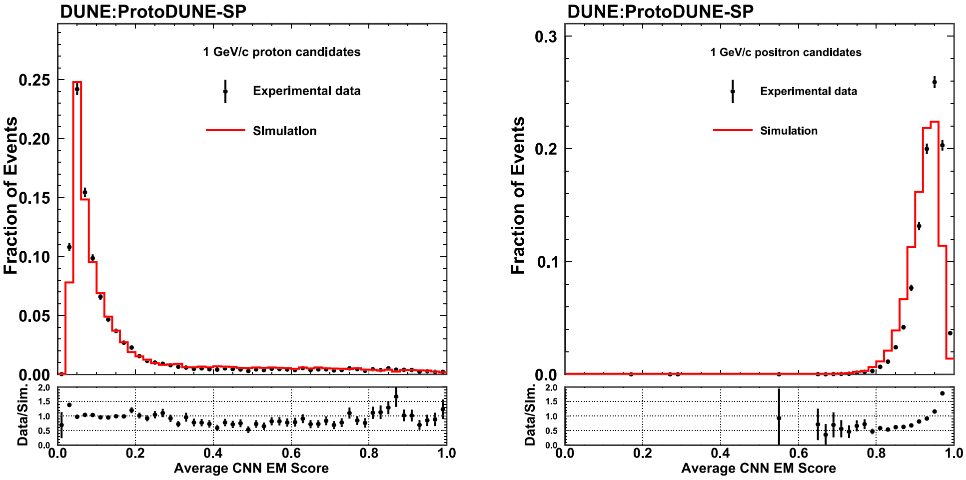

(c) proton **(d)** positron

Table 4 Fraction of reconstructed particles classified into appropriate class for different samples in ProtoDUNE-SP data and simulation. The errors represent the statistical uncertainties calculated using the Clopper–Pearson method [29]

Hit source	Class	Data fraction (%)	Simulation fraction (%)	Data/simulation
Pion	Track	91.7 ± 0.4	92.5 ± 0.2	0.991 ± 0.005
Muon	Track	$100^{+0.0}_{-0.1}$	$100^{+0.0}_{-0.1}$	$1.000^{+0.000}_{-0.002}$
Proton	Track	96.9 ± 0.2	97.1 ± 0.1	0.998 ± 0.002
Positron	Shower	98.8 ± 0.1	97.9 ± 0.1	1.010 ± 0.001

to which the results from the CNN can be compared. For simulation samples we use the truth information to get the primary beam particle species information. This allows the shower score distributions from the CNN to be compared between experimental data and simulation for different particle species. The reconstructed particles with angles inconsistent with the beam direction and that arrive out-of-time with the beam can be assumed to be cosmic muons. Note that at 1 GeV/c beam momentum, π^+ and μ^+ are indistinguishable using the beam instrumentation information. A 1 GeV/c μ^+ is expected to stop in the middle of the detector around z = 380 cm, where the z axis is horizontal. A 1 GeV/c π^+ will most likely interact with the argon nucleus before stopping because of the relatively short interaction length ($\sim$ 100 cm). We identify an event as a pion if the reconstructed track end z position is less than 100 cm and as a muon if the end z position is greater than 300 cm for events identified by the beam instrumentation as either pions or muons. We require the number of collection plane hits in the reconstructed shower should be greater than 200 for the positron candidate events in order to remove events with an incompletely reconstructed shower. This cut is not applied to the other three particle species. Table 2 shows the numbers of events after the beam quality and number of hits cuts for beam pions, muons, protons and positrons and the purity of the selected samples based on the truth information in the simulation.

Figure 11 shows the distribution of shower classifier score for each individual hit in the beam pions, muons, protons, and positrons. The data in all of the beam particle distributions are normalised by the number of triggered beam particles of the given flavour after the beam quality and number of hits cuts. There is a reasonable agreement between the experimental data and simulation in terms of the shower score distributions for each particle species. To quantify the efficiency to select track-like and shower-like hits, Table 3 lists the fraction of individual hits selected into the appropriate category for each sample in experimental data and simulation for a selection threshold of 0.72. The difference between the selected fraction in each case is an estimate of the systematic uncertainty associated with hit-by-hit selection. The class used for the selection in each sample is also given in Table 3. The fractional difference between experimental data and simulation varies based on the particles species, and falls in the range of 1–2%.

Figure 12 shows the distribution of the average shower classifier scores over all the hits in the reconstructed pion, proton, and positron particles. This average shower classifier score is what analysers normally use to identify a reconstructed particle as a track-like or shower-like particle. The distributions in each category are normalised to unit area. The experimental data and simulation distributions are in a reasonable agreement. There is a long tail in the average shower classifier score distribution for both the beam pions and protons. This tail is caused by the spatial distortion introduced by the SCE and is largely suppressed if we make the distributions using simulation sample without simulating SCE. There is a shift in the average shower classifier score for beam positrons between experimental data and simulation. There are slightly more hits in experimental data than in simulation for reconstructed positron events, making the experimental data hits more shower-like. It can be seen that the score distribution for the beam muons is more strongly peaked towards low scores than for cosmic-ray muons, shown in Fig. 10, because they are significantly lower in energy and hence produce fewer delta rays. Table 4 lists the fraction of reconstructed particles selected into the appropriate category for each sample in experimental data and simulation for a selection threshold of 0.81. The fractional difference between experimental data and simulation is within 1% for all particles species.

3.3 Michel electrons

To validate the performance of the CNN Michel score calculation, we examine the Michel score of hits around the muon and pion track end point. Hits around the muon end points are most likely from the Michel electron which are expected to have a high Michel score. We define a window of 30 wires $\times$ 200 ticks (approximately 15×16 cm^2) centred around the reconstructed track end point projected on the collection plane to select daughter hits. Hits from the secondary particles produced by the pion interaction are expected to have a low Michel score as shown in Fig. 13a. The Michel hits from the muon decay are expected to have a high Michel score as shown in Fig. 13b. Hits on the primary beam track or on another track that is longer than 25 cm are excluded to remove the contributions from primary beam particle and cosmic ray muons. Figures 14 and 15 show the hit-level and particle level comparison of the CNN Michel score over daughter hits in the reconstructed pion and muon particles.

The results of the hit-level and event-level classification, obtained using a threshold of 0.19, are given in Tables 5 and 6, respectively. The threshold is chosen to maximise the product of selection efficiencies of pions and muons. We are able to select 73% of the μ^+ events while rejecting 90–92% of the π^+ events using the average Michel score. The fractional difference between experimental data and simulation falls in the range of 1–2%. Efficient identification of Michel electrons provides crucial information on particle identification and kinematic reconstruction. It allows the separation between μ^+ and μ^- because 70% of the μ^-s are captured while most of the μ^+s decay into Michel electrons. It also allows the identification of stopping π^+ which goes through the decay chain $\pi^+ \rightarrow \mu^+ \rightarrow e^+$. The momentum of those stopping pions can be reconstructed either through track range or using calorimetric information, which can be used to reconstruct the full kinematics of the final state particles.

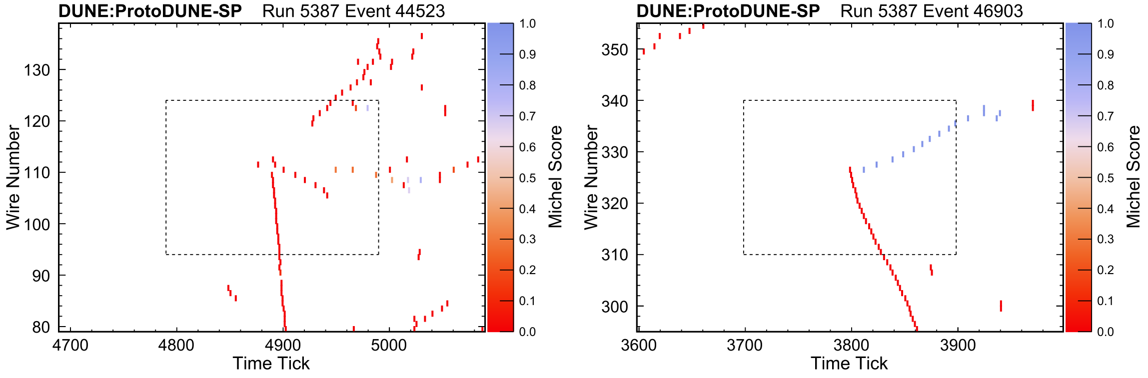

(a) A pion candidate **(b)** A muon candidate

Fig. 13 CNN Michel score for reconstructed primary beam particles and secondary particles in a reconstructed pion (left) and muon (right) particle. Each coloured pixel shows the peak time and wire number of a hit. The box surrounding the track end point is used to select the daughter hits. The average daughter Michel score is 0.005 for the pion event and 1.000 for the muon event

Fig. 14 CNN Michel score for the daughter hits in the 30 wires × 200 ticks window centred around the reconstructed track end point of the pion (left) and muon (right) particles

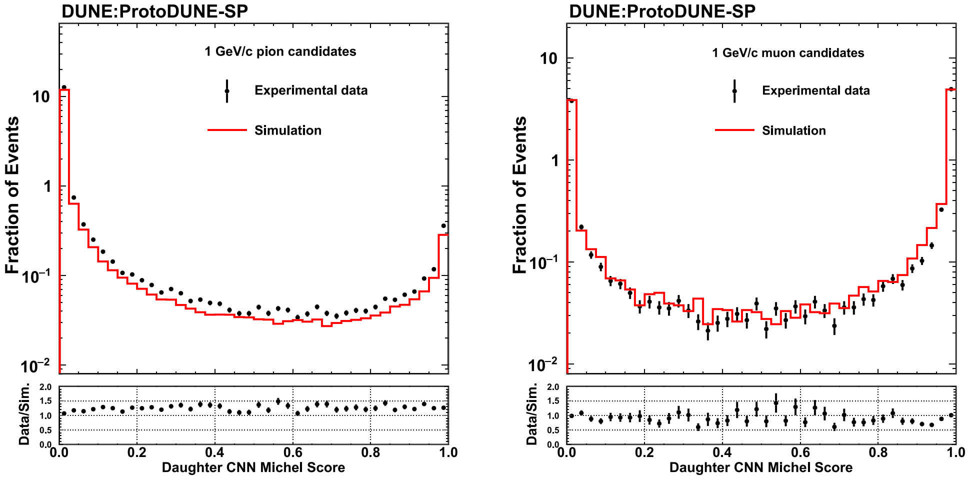

(a) Pion candidates **(b)** Muon candidates

Fig. 15 Average CNN Michel score over the daughter hits in the 30 wires × 200 ticks window centred around the reconstructed track end point of the pion (left) and muon (right) particles

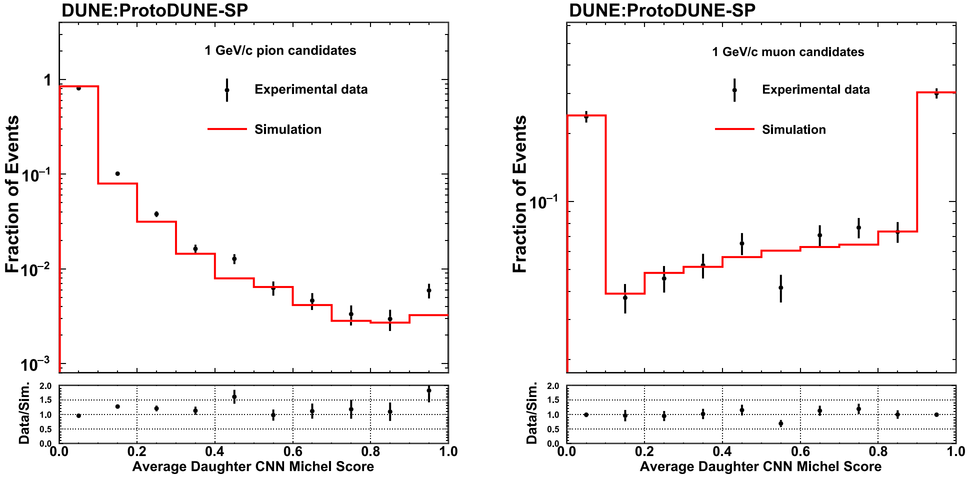

(a) Pion candidates **(b)** Muon candidates

Table 5 Fraction of daughter hits classified into appropriate class for different samples in ProtoDUNE-SP data and simulation. The statistical uncertainties on the fractions and ratios are negligible

Hit source	Class	Data fraction (%)	Simulation fraction (%)	Data/simulation
Pion daughters	Non-Michel-like	87.6	89.2	0.982
Muon daughters	Michel-like	59.8	60.2	0.993

Table 6 Fraction of reconstructed particles classified into appropriate class for different samples in ProtoDUNE-SP data and simulation. The errors represent the statistical uncertainties calculated using the Clopper–Pearson method [29]

Hit source	Class	Data fraction (%)	Simulation fraction (%)	Data/simulation
Pion daughters	Non-Michel-like	90.4 ± 0.4	92.2 ± 0.2	0.980 ± 0.005
Muon daughters	Michel-like	73.2 ± 1.3	72.6 ± 1.3	$1.009^{+0.025}_{-0.026}$

4 Conclusion

In this paper, we described an effective hit tagging algorithm for track, shower, and Michel electron hit classification based on a convolutional neural network, using a small patch approach. This algorithm is shown to give good agreement in selection efficiencies, of around 1–2%, between experimental data and simulation for cosmic rays and 1 GeV/c test-beam interactions for a hit-by-hit event selection. When combined with the full event reconstruction (which includes a BDT-based classifier) and applied to the hits of each reconstructed particle, the CNN refines the track and shower classification to produce highly efficient selections that agree within 1% between experimental data and simulation. Additionally, this network also provides a method to select Michel electrons, which helps with the particle identification and kinematic reconstruction. This algorithm is being widely used within ongoing ProtoDUNE-SP data analyses, including pion cross-section analyses and detector calibrations.

Acknowledgements The ProtoDUNE-SP detector was constructed and operated on the CERN Neutrino Platform. We gratefully acknowledge the support of the CERN management, and the CERN EP, BE, TE, EN and IT Departments for NP04/ProtoDUNE-SP. This document was prepared by the DUNE collaboration using the resources of the Fermi National Accelerator Laboratory (Fermilab), a U.S. Department of Energy, Office of Science, HEP User Facility. Fermilab is managed by Fermi Research Alliance, LLC (FRA), acting under Contract No. DE-AC02-07CH11359. This work was supported by CNPq, FAPERJ, FAPEG and FAPESP, Brazil; CFI, IPP and NSERC, Canada; CERN; MŠMT, Czech Republic; ERDF, H2020-EU and MSCA, European Union; CNRS/IN2P3 and CEA, France; INFN, Italy; FCT, Portugal; NRF, South Korea; CAM, Fundación "La Caixa", Junta de Andalucía-FEDER, MICINN, and Xunta de Galicia, Spain; SERI and SNSF, Switzerland; TÜBİTAK, Turkey; The Royal Society and UKRI/STFC, United Kingdom; DOE and NSF, United States of America. This research used resources of the National Energy Research Scientific Computing Center (NERSC), a U.S. Department of Energy Office of Science User Facility operated under Contract No. DE-AC02-05CH11231.

Data Availability Statement This manuscript has no associated data or the data will not be deposited. [Authors' comment: The CNN described in this paper classifies low-level data and does not directly produce physics results, hence there is no associated data release.]

Funded by SCOAP^3. SCOAP^3 supports the goals of the International Year of Basic Sciences for Sustainable Development.

References

1. B. Abi et al., First results on ProtoDUNE-SP liquid argon time projection chamber performance from a beam test at the CERN Neutrino Platform. JINST **15**(12), P12004 (2020)
2. A. Abed Abud et al., Design, construction and operation of the ProtoDUNE-SP Liquid Argon TPC. JINST **17**(01), P01005 (2022)
3. B. Abi et al., Volume I. Introduction to DUNE. JINST **15**(08), T08008 (2020)
4. B. Abi et al., Volume IV. The DUNE far detector single-phase technology. JINST **15**(08), T08010 (2020)
5. N. Charitonidis, I. Efthymiopoulos, Low energy tertiary beam line design for the CERN neutrino platform project. Phys. Rev. Accel. Beams **20**, 111001 (2017)
6. A.C. Booth, N. Charitonidis, P. Chatzidaki, Y. Karyotakis, E. Nowak, I. Ortega-Ruiz, M. Rosenthal, P. Sala, Particle production, transport, and identification in the regime of 1–7 GeV/c. Phys. Rev. Accel. Beams **22**(6), 061003 (2019)
7. A. Reynolds, *Evaluating the low-energy response of the ProtoDUNE-SP detector using Michel electrons*. PhD thesis (University of Oxford, 2020)
8. L. Michel, Interaction between four half spin particles and the decay of the μ meson. Proc. Phys. Soc. A **63**, 514–531 (1950)

9. J.S. Marshall, M.A. Thomson, The Pandora software development kit for pattern recognition. Eur. Phys. J. C **75**(9), 439 (2015)
10. R. Acciarri et al., The Pandora multi-algorithm approach to automated pattern recognition of cosmic-ray muon and neutrino events in the MicroBooNE detector. Eur. Phys. J. C **78**(1), 82 (2018)
11. A. Abed Abud et al., Reconstruction of interactions in the ProtoDUNE-SP detector with Pandora
12. A. Aurisano, A. Radovic, D. Rocco, A. Himmel, M.D. Messier, E. Niner, G. Pawloski, F. Psihas, A. Sousa, P. Vahle, A convolutional neural network neutrino event classifier. JINST **11**(09), P09001 (2016)
13. R. Acciarri et al., Convolutional neural networks applied to neutrino events in a liquid argon time projection chamber. JINST **12**(03), P03011 (2017)
14. B. Abi et al., Neutrino interaction classification with a convolutional neural network in the DUNE far detector. Phys. Rev. D **102**, 092003 (2020)
15. C. Adams et al., Deep neural network for pixel-level electromagnetic particle identification in the MicroBooNE liquid argon time projection chamber. Phys. Rev. D **99**(9), 092001 (2019)
16. F. Psihas, E. Niner, M. Groh, R. Murphy, A. Aurisano, A. Himmel, K. Lang, M.D. Messier, A. Radovic, A. Sousa, Context-enriched identification of particles with a convolutional network for neutrino events. Phys. Rev. D **100**, 073005 (2019)
17. R. Abbasi et al., A convolutional neural network based cascade reconstruction for the IceCube Neutrino Observatory. JINST **16**, P07041 (2021)
18. L.D. Jackel, R.E. Howard, B. Boser, J.S. Denker, D. Henderson, Y. LeCun, W. Hubbard, Backpropagation Applied to Handwritten Zip Code Recognition (2008)
19. C. Szegedy, W. Liu, Y. Jia, P. Sermanet, S. Reed, D. Anguelov, D. Erhan, V. Vanhoucke, A. Rabinovich, Going deeper with convolutions. In *Proceedings of the IEEE Computer Society Conference on Computer Vision and Pattern Recognition* (2015)
20. E.D. Church, LArSoft: a software package for liquid argon time projection drift chambers. arXiv:1311.6774 [physics.ins-det] (2013)
21. M. Wang, T. Yang, M.A. Flechas, P. Harris, B. Hawks, B. Holzman, K. Knoepfel, J. Krupa, K. Pedro, N. Tran, GPU-accelerated machine learning inference as a service for computing in neutrino experiments. Front. Big Data **3**, 48 (2021)
22. S. Palestini, Space charge effects in noble liquid calorimeters and time projection chambers. Instruments **5**(1), 9 (2021)
23. N. Srivastava et al., Dropout: a simple way to prevent neural networks from overfitting. J. Mach. Learn. Res. **15**, 1929–1958 (2014)
24. C. Nwankpa, W. Ijomah, A. Gachagan, S. Marshall, Activation functions: Comparison of trends in practice and research for deep learning. arXiv:1811.03378 [cs.LG] (2018)
25. M. Abadi, P. Barham, J. Chen, Z. Chen, A. Davis, J. Dean, M. Devin, S. Ghemawat, G. Irving, M. Isard et al., Tensorflow: a system for large-scale machine learning. OSDI **16**, 265–283 (2016)
26. F. Chollet et al., Keras. https://keras.io (2015)
27. https://www.tensorflow.org/tensorboard
28. L. Prechelt, *Early Stopping—But When?* (Springer, Berlin, 2012), pp.53–67
29. C.J. Clopper, E.S. Pearson, The use of confidence or fiducial limits illustrated in the case of the binomial. Biometrika **26**(4), 404–413 (1934)